Electronic Supplementary Material (ESI) for RSC Advances.

Supplementary Information

Tailoring spatial distribution of $Eu(TTA)_3phen$ within electrospun polyacrylonitrile nanofibers for high fluorescence efficiency

Ying Li, Chun-Yan Zhang, Deng-Guang Yu,* Xia Wang*

School of Materials Science & Engineering, University of Shanghai for Science and Technology, Shanghai 200093, China

*** Corresponding authors:**
E-mail: ydg017@usst.edu.cn (DG Yu); wangxia@usst.edu.cn (X Wang)

Setting up the electrospinning system

Shown in Fig. S1 is an electrospinning system that consists of two syringe pumps, a homemade concentric spinneret, a fiber collector and a high power supply. The collector plate was simply prepared from a flat piece of cardboard wrapped with aluminum foil and was grounded. A KDS100 syringe pump (Cole-Parmer®, Vernon Hills, USA) were used to drive the sheath fluid. A KDS200 syringe pump (Cole-Parmer®, Vernon Hills, USA) were used to drive the core solution. A ZGF 60kV/2mA power supply (Shanghai Sute Corp., Shanghai, China) was employed to provide a potential difference between the spinneret and collector. An alligator clip connected the concentric spinneret to the power supply. The collector was kept at a fixed distance of 20 cm from the needle tip of the spinneret. The coaxial processes were recorded using a digital video recorder (PowerShot A640, Canon, Japan) under 12×magnification.

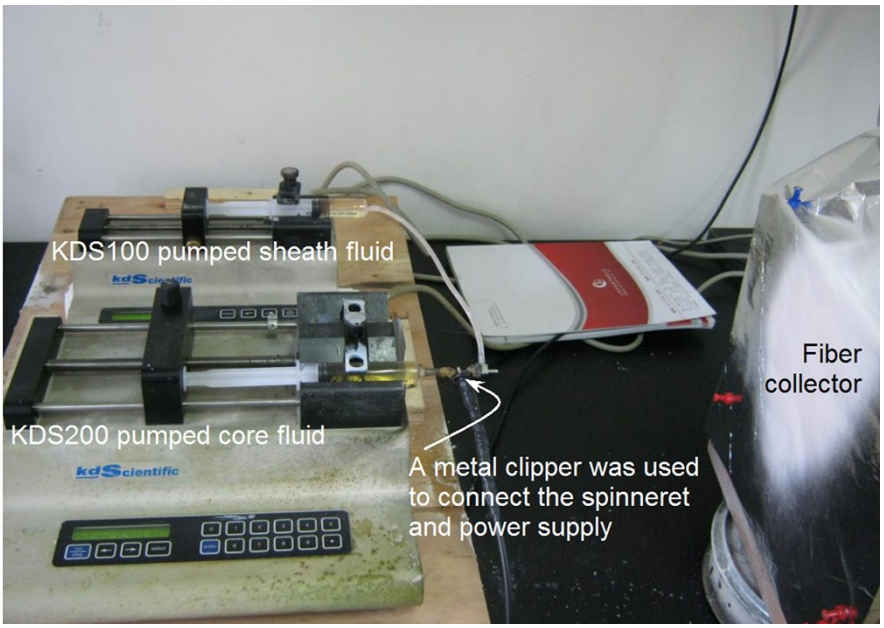

Fig. S1 The arrangement of the apparatus for electrospinning.

Observations of the coaxial processes

Photographs of the electrospinning of of N3 using the standard coaxial process and of the modified coaxial electrospinning of N5 and N6 are given in Fig. S2. In all these processes, a typical fluid jet trajectory could be observed with a straight thinning jet emitted from a compound Taylor cone, followed by an unstable bending and whipping region with loops of increasing size. However, several differences can be seen between the traditional and modified coaxial processes. The compound Taylor cone in the traditional process had a conical shape (inset of Fig. S2a), but those in the modified coaxial process could not be distinguished due to their retraction into the concentric spinneret (insets of Fig. S2b and S2c). The different surface tensions of the $Eu(TTA)_3$phen solutions and PAN fluids resulted in these differences. And the bending and whipping regions (Fig. S2b and S2d) in the modified coaxial process

were more colorful than those in the traditional coaxial process owing to the presence of Eu(TTA)$_3$phen in the sheath fluid (Fig. S2a).

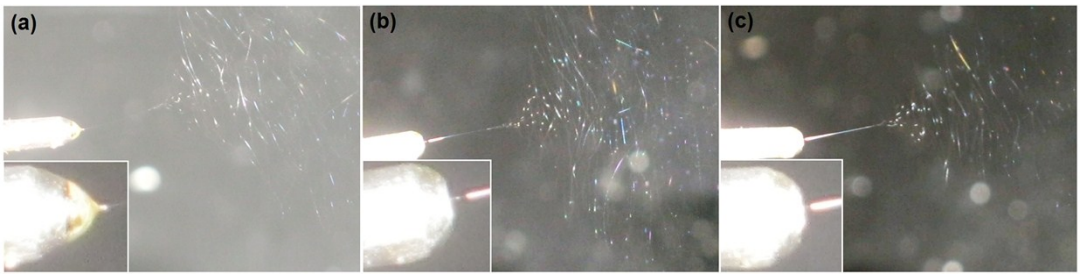

Fig. S2 Digital images of the electrospinning processes for preparing fibers N3 (a), N5 (b) and N6 (c); the insets are the corresponding Taylor cones under an applied voltage of 18 kV.

EDS results for fibers N3 and N5

EDS results for the fibers N3 and N5 are presented in Fig. S3. The contents of Eu are 0.59% and 0.64% by weight, respectively. The theoretical content of Eu^{3+} in these fibers can be calculated from the operational parameters. Element Eu^{3+} has an atomic weight of 152.0 and Eu(TTA)$_3$phen has a molecular weight of 1016.76, thus the theoretical Eu content in both fibers is {(152/1016.76)×(0.2×2.5%)/[(0.2×2.5%)+(0.8×15%)]}×100% = 0.60%, in agreement with the observed values. The EDS date hence demonstrate that all the Eu(TTA)$_3$phen complexes were successfully encapsulated in the core of N3 or coated on the surface of N5.

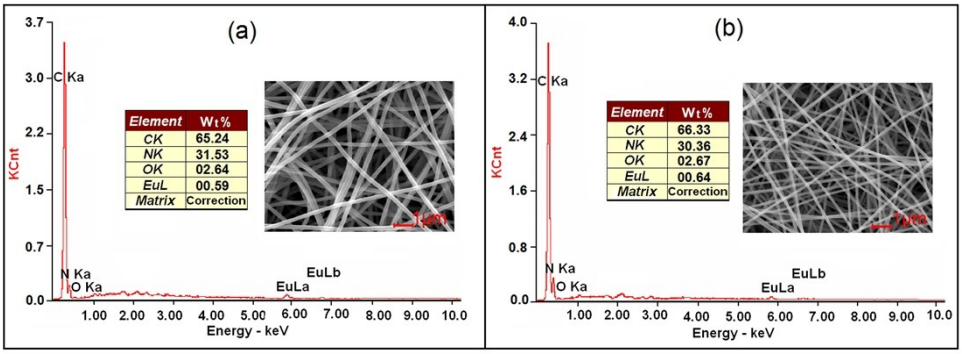

Fig. S3. EDS spectra of fibers N3 from traditional coaxial electrospinning (a) and N5 from the modified coaxial process (b).

Determinations of the Emission Quantum Efficiency (η)

The quantum efficiency of the luminescence step, η expresses how well the radiative processes (characterized by rate constant A_r) compete with non-radiative processes (overall rate constant A_{nr}) . Assuming that only nonradiative and radiative processes are involved in the depopulation of the $^5D_0$ statea, η can be defined as

follows:[S1]

$$A_r + A_{nr} \quad (1)$$

A_r can also be obtained by summing over the radiative rates A_{0J} for each $^5D_0 \rightarrow {}^7F_J$ (J=0-4) transitions of Eu^{3+}.

$$A_r = \Sigma A_{0J} = A_{00} + A_{01} + A_{02} + A_{03} + A_{04} \quad (2)$$

The branching ratio for the $^5D_0 \rightarrow {}^7F_{5,\,6}$ transitions can be neglected as they are not detected experimentally, and so their influence can be ignored in the depopulation of the $^5D_0$ excited state. Since $^5D_0 \rightarrow {}^7F_1$ is an isolated magnetic dipole transition, it is practically independent of the chemical environment around the Eu^{3+} ion, and thus can be considered as an internal reference for the whole spectrum. As a result, the experimental coefficients of spontaneous emission, A_{0J} can be calculated according to the equation.[S2, S3]

$$A_{0J} = A_{01}(I_{0J}/I_{01})(v_{01}/v_{0J}) \quad (3)$$

Here, A_{0J} is the experimental coefficient of spontaneous emission. A_{01} is the Einstein's coefficient of spontaneous emission between the $^5D_0$ and $^7F_1$ energy levels. In vacuum, A_{01} has a value of 14.65 s^{-1}, and if an average index of refraction n equal to 1.506 is assumed, the value of A_{01} can be determined to be approximately 50 s^{-1} ($A_{01} = n^3 A_{01\,(vac)}$).[S4] I_{01} and I_{0J} are the integrated intensities of the $^5D_0 \rightarrow {}^7F_1$ and $^5D_0 \rightarrow {}^7F_J$ transitions (J = 0-4) with v_{01} and v_{0J} ($v_{0J} = 1/\lambda_J$) energy centers respectively. υ_{0J} refers to the energy barrier and can be determined from the emission bands of Eu^{3+}'s $^5D_0 \rightarrow {}^7F_J$ emission transitions. The emission intensity, I, taken as integrated intensity S of the $^5D_0 \rightarrow {}^7F_{0\text{-}4}$ emission curves, can be defined as below:

$$I_{i\text{-}j} = \hbar \omega_{i\text{-}j} A_{i\text{-}j} N_i \approx S_{i\text{-}j} \quad (4)$$

where i and j are the initial ($^5D_0$) and final levels ($^7F_{0\text{-}4}$), respectively, $\omega_{i\text{-}j}$ is the transition energy, $A_{i\text{-}j}$ is the Einstein's coefficient of spontaneous emission, and N_i is the population of the $^5D_0$ emitting level. On the basis of reference,[S5-S9] the value of $A_{01} \approx 50$ s^{-1} and the lifetime (τ), radiative (A_r), and nonradiative (A_{nr}) transition rates are related through the following equation:

$$\tau_{exp} = (A_r + A_{nr})^{-1} \quad (5)$$

On the basis of the above discussion, the quantum efficiencies of the nanofiber materials can be determined, as shown in Table 2. From the equation for η, it can be seen the value η mainly depends on the values of two quanta: one is lifetimes and the other is I_{02} / I_{01}. Furthermore, we determined the Judd-Ofelt Parameters for the pure complex $Eu(TTA)_3phen$ and nanofibers. The spontaneous emission probability, A, of the transition is related to its dipole strength according to eqn. (6).[S10-S13]

$$A = (64\pi^4 \upsilon^3)/[3h(2J+1)]\{[(n^2+2)^2/9n]S_{(ED)} + n^2 S_{(MD)}\} \quad (6)$$

υ is the average transition energy in cm^{-1}, h is Planck constant, $2J+1$ is the degeneracy of the initial state (1 for $^5D_0$). $S_{(ED)}$ and $S_{(MD)}$ are the electric and magnetic dipole strengths, respectively. The factors containing the medium's refractive index n result from local field corrections that convert the external electromagnetic field into an effective field at the location of the active center in the dielectric medium. All the transitions from $^5D_0$ to $^7F_{0,\,3,\,5}$ (J = 0, 3, 5) are forbidden both in magnetic and induced electric dipole schemes ($S_{(ED)}$ and $S_{(MD)}$ are zero). The transition from $^5D_0$ to to $^7F_1$ (J = 1) is the isolated magnetic dipole transition and has no electric dipole contribution,

and thus it is practically independent of the ion's chemical environment and can be used as a reference as mentioned above. In addition, the $^5D_0 \rightarrow {}^7F_6$ transition could not be experimentally detected and so it is not necessary to determine its J-O parameter. Hence, we only need to estimate the two parameters (Ω_2, Ω_4) related to the two purely induced electric dipole transitions $^5D_0 \rightarrow {}^7F_{2,4}$ on basis of only three parameters Ω_λ using eqn. (7): [S11, S14]

$$A = (64e^2\pi^4\upsilon^3)/[3h(2J+1)]\{[(n^2+2)^2/9n]\Sigma\Omega_\lambda|\langle J||U^{(\lambda)}||J'\rangle|^2 \quad (7)$$

e is the electronic charge. With the refraction index n = 1.506,[S15] and $|\langle J||U^{(\lambda)}||J'\rangle|^2$ values are the square reduced matrix elements whose values are 0.0032 and 0.0023 for J = 2 and 4, respectively. The Ω_2, Ω_4 intensity parameters for all the samples are shown in Table 2. It can be seen that the fibers have relatively high values for the Ω_2 intensity parameter. This might be interpreted as being the consequence of the hypersensitive behavior of the $^5D_0 \rightarrow {}^7F_2$ transition, indicating that the Eu^{3+} ion is located in a polarizable chemical environment for luminescence.

Table S1 Photoluminescent data of $Eu(TTA)_3phen$ and electrospun nanofibers.

Materials	$Eu(TTA)_3phen$	N2	N4	N5
ν_{00} (cm_{-1})	17238	17299	17299	17317
ν_{01} (cm^{-1})	16940	16951	16951	16983
ν_{02} (cm^{-1})	16329	16370	16370	16399
ν_{03} (cm^{-1})	15328	15373	15373	15373
ν04 (cm-1)	14235	14256	14233	14245
I_{01}	210.31	6921.96	5934.77	20253.35
I_{02}	1023.12	103986.61	101368.67	239618.52
I_{02}/I_{01}	4.86	15.02	17.08	11.83
A_{00} (s^{-1})	15.99	56.23	36.30	22.81
A_{01} (s^{-1})	50	50	50	50
A_{02} (s^{-1})	252.34	777.79	884.33	612.62
A_{03} (s^{-1})	7.51	20.76	23.64	17.35
A_{04} (s^{-1})	6.31	27.91	35.00	27.73
τ (ms)	0.80	0.62	0.60	0.77
$1/\tau(s^{-1})$	1250	1610	1670	1300
A_r	332.15	932.69	1029.27	833.32
A_{nr}	917.85	677.31	640.73	466.68
η (%)	26.57	57.93	61.63	64.10
Ω_2 （$\times 10^{-20} cm^2$）	7.31	22.54	25.63	17.76
Ω_4 （$\times 10^{-20} cm^2$）	0.42	1.86	2.33	1.85

References

s1 Q. Li, T. Li and J.G. Wu, *J. Phys. Chem. B,* 2001,**105**, 12293.

s2 P.C.R. Soares-Santos, H.I.S. Nogueira, V. Félix, M.G. . Drew, R.A. Sá Ferreira,

L.D. Carlos and T. Trindade, *Chem*. *Mater*., 2003, **15**, 100.
s3 L. Guo, L.S. Fu, R.A.S. Ferreira, L.D. Carlos, Q.P. Li and B. Yan, *J. Mater. Chem.*, 2011, **21**, 15600.
s4 L.D. Carlos, Y. Messaddeq, H.F. Brito, R.A. Sá Ferreira, V. de Zea Bermudez and S.J.L. Ribeiro, *Adv*. *Mater*., 2000, **12**, 594.
s5 H.R. Li, D. Li, Y.G. Wang, Q.R. Ru, *Chem-Asian J.,* 2011, **6**, 1443.
s6 J.C. Boyer, F. Vetrone, J.A. Capobianco, A. Speghini and M. Bettinelli, *J*. *Phys*. *Chem*. *B*., 2004, **108**, 20137.
s7 S.T. Frey, M.L. Gong and Jr. W.D. Horrocks, *Inorg*. *Chem*., 1994, **33**, 3229.
s8 O.L. Malta, H.J. Batista and L.D. Carlos, *Chem*. *Phys*., 2002, **282**, 21.
s9 K. Binnemans, P. Lenaerts, K. Driesen and C. Görller-Walrand, *J. Mater. Chem*., 2004, **14**, 191.
s10 H.R. Li, J. Lin, H.J. Zhang, L.S. Fu, Q.G. Meng and S.B. Wang, *Chem. Mater*., 2002, **14**, 3651.
s11 O.L. Malta, H.F. Brito, J.F.S. Menezes, F.R. Gonçalvese Silva, Jr. Alves, S., Jr. Farias and F.S.A.V.M. Andrade, *J*. *Lumin*. 1997, **75**, 255.
s12 G.F. de Sa´, O.L. Malta, C. de Mello Donega´, A.M. Simas, R.L. Longo, P. . Santa-Cruz and Jr. da Silva, E. F., *Coord*. *Chem*. *Rev*., 2000, **196**, 165.
s13 A. Kodaira, A. Claudia, H.F. Brito and M.C.F.C. Felinto, *J*. *Solid State Chem*., 2003, **171**, 401.
s14 K. Binnemans, K. Van Herck and C. Görller-Walrand, *Chem*. *Phys. Lett*., 1997, **266**, 297.
s15 L.N. Sun, H.J. Zhang, C.Y. Peng, J.B. Yu, Q.G. Meng, L.S. Fu, F.Y. Liu and X.M. Guo, *J. Phys. Chem. B*, 2006, **110**, 7249.